

Old star clusters: Bench tests of low mass stellar models

M. Salaris^a

Astrophysics Research Institute, Liverpool John Moores University, 12 Quays House, Birkenhead CH41 1LD, UK

Abstract. Old star clusters in the Milky Way and external galaxies have been (and still are) traditionally used to constrain the age of the universe and the timescales of galaxy formation. A parallel avenue of old star cluster research considers these objects as bench tests of low-mass stellar models. This short review will highlight some recent tests of stellar evolution models that make use of photometric and spectroscopic observations of resolved old star clusters. In some cases these tests have pointed to additional physical processes efficient in low-mass stars, that are not routinely included in model computations. Moreover, recent results from the *Kepler* mission about the old open cluster NGC6791 are adding new tight constraints to the models.

1. INTRODUCTION

Resolved old star clusters (globular and old open clusters) have been traditionally employed to estimate a lower limit for the age of the universe, determine the formation timescale of the Galactic halo (i.e. [33],[30]) and the time-delay between halo and disk formation (i.e., [32]). They can in principle also (weakly) constrain the baryonic mass density of the universe from the determination of the initial He-abundance in globular cluster stars (i.e., [13]) or their initial Li abundance. Unresolved old star clusters in external galaxies are also routinely employed to constrain the early stages of the star formation history of the host galaxies, by determining ages and initial metallicities from their integrated colours/spectra ([25]).

Here it is adopted the ‘evolutionary’ definition of ‘old’, i.e. clusters are denoted as ‘old’ when they are populated by stars that produce an electron degenerate He-core at the end of the Main Sequence (MS). In terms of Colour-Magnitude-Diagrams (CMDs) these clusters show a well developed Red Giant Branch (RGB). Their age is older than ≈ 1 Gyr. Resolved old star clusters, and in particular the well populated globular clusters (GCs) of the Milky Way and the old clusters in the neighbouring Magellanic Clouds, are a formidable test bench for stellar evolution models of low mass stars. The next sections present a brief summary of some recent tests for stellar evolution models driven by photometric and spectroscopic observations of resolved, old star clusters.

2. PHOTOMETRIC DIAGNOSTICS

Photometry of large sample of stars produces CMDs and Luminosity Functions (LFs – star counts as a function of magnitude) that are compared to the corresponding predictions of theoretical isochrones, to highlight (in)consistencies between theory and observations. The common wisdom that GCs are simple stellar populations (SSPs) made of stars with the same age and initial chemical composition

^ae-mail: ms@astro.livjm.ac.uk

has been recently shattered by observations of CNO_{Na} (and sometimes also MgAl) anticorrelations among stars within individual clusters (see, i.e., [10]). These observations are commonly interpreted in terms of multiple (quasi-coeval) generations of stars born out of primordial matter polluted by the winds of either massive AGB or fast rotating massive first generation stars (see, i.e., [27]). As a byproduct of these processes, one expects that also the He-abundance varies to some degree amongst stars in individual clusters. This undoubtedly makes the use of some observations for stellar model-testing more problematic.

2.1 RGB effective temperature

Due to the roughly ‘vertical’ nature of the RGB in bolometric magnitude- T_{eff} diagrams (that minimises the effect of uncertainties in distance moduli), and the independence of its location on age for old populations, T_{eff} estimates for RGB stars in Galactic GCs have been since long used to test the adequacy for more advanced evolutionary phases (and different initial chemical compositions) of the solar calibration of the free parameter a_{ml} in the mixing length theory (MLT), used to calculate the temperature gradient in superadiabatic convective regions (see, i.e. [31]).

In fact, besides a_{ml} there are 3 additional free parameters entering the MLT that are generally fixed a priori, before the calibration of a_{ml} . These three parameters – that determine the MLT ‘flavour’ – plus a_{ml} enter the equations that determine v_c , the average convective flux F_c and the convective efficiency Γ at each point within a convective region. Once these parameters are fixed, the temperature gradient and the resulting T_{eff} , depend on the value of a_{ml} . On the other hand, when a_{ml} is kept fixed and one or more of the other three parameters are varied, the temperature gradients and T_{eff} are also affected.

Figure 1 displays a comparison between the average T_{eff} at $M_{\text{bol}} = -3$ for a sample of Galactic GCs ([16]), and theoretical models calculated with a solar-calibrated a_{ml} for two different ‘flavours’ of the MLT ([29]). The dashed line displays models with the ‘standard flavour’ (BV58) of the MLT used in stellar evolution models ([8]), whereas the solid line displays models with the MLT flavour usually employed in WD model atmosphere calculations (MLT2). The value of solar calibrated a_{ml} is very different between the two cases (a difference by a factor ~ 3) but the two sets of predictions are very similar, with differences of only ~ 50 K, and are both generally consistent with the empirical T_{eff} estimates.

2.2 RGB bump

The bump appearing in LF of RGB stars in GCs is produced by the encounter of the H-burning shell with the H-abundance discontinuity left over by the outer convection at its maximum depth, reached during the first dredge-up. The sharp increase in the H-abundance causes an abrupt decrease of the mean molecular weight (μ), that affects the efficiency of the H-burning shell, proportional to a high power of μ . This occurrence causes a temporary drop in the surface luminosity, before this starts to increase again. As a consequence, a low-mass RGB star crosses the same luminosity interval three times, and a bump (a local maximum) appears in the RGB LF, as shown in Fig. 2. Given that the RGB-bump brightness depends on the maximum depth attained by the convective envelope, and on the chemical profile above the advancing H-burning shell, the comparison between predicted and observed RGB-bump magnitudes provides valuable information about the internal structure of low-mass stars during their RGB evolution.

The observational parameter routinely adopted to test the theoretical predictions of the RGB bump brightness is the V-magnitude (or similar band-passes) difference between the RGB-bump and the Horizontal Branch (HB) at the RR Lyrae instability strip level, $\Delta V_{\text{HB}}^{\text{bump}}$. This has the advantage of being formally independent of distance and reddening, but it is affected by uncertainties in the placement of the observed HB level for GCs with blue HB morphologies, and in theoretical predictions of the HB luminosity. Comparisons of observed and theoretical $\Delta V_{\text{HB}}^{\text{bump}}$ values have in the past provided conflicting results about the adequacy of standard stellar evolution models (see, i.e., [17] and [11] for opposite

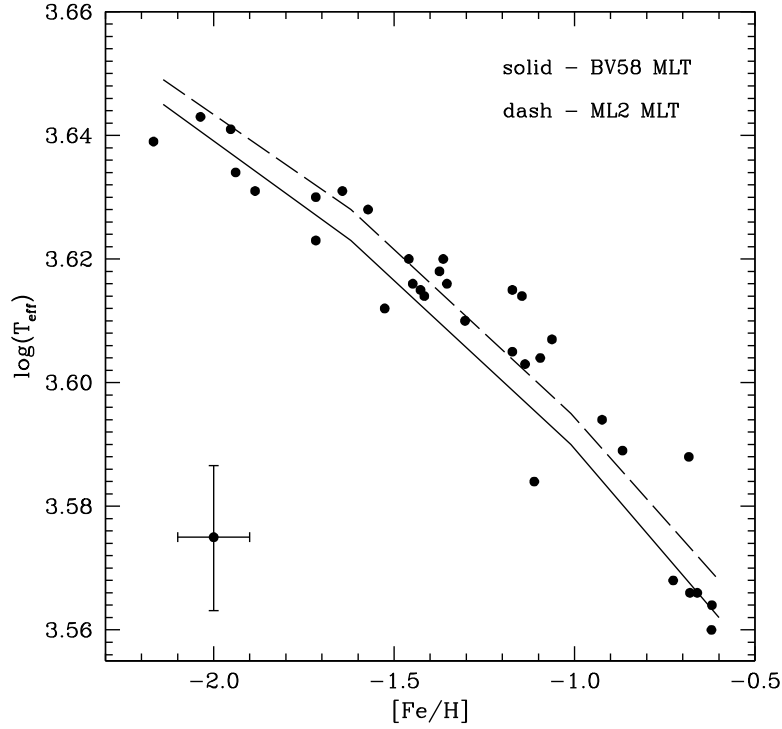


Figure 1. Estimates of the average RGB T_{eff} at $M_{\text{bol}} = -3$ for a sample of Galactic GCs (the typical error bars are also displayed), compared to the corresponding values from models with two different ‘flavours’ of the mixing length theory.

conclusions). An alternative avenue explored recently ([14]) is offered by the magnitude difference between the MS Turn Off (TO) and the RGB-bump brightness $\Delta V_{\text{TO}}^{\text{Bump}}$. The values predicted by theoretical models for cluster ages estimated from the TO absolute magnitudes, are larger than observed in a small sample of well populated clusters with accurate photometry, as shown in Fig. 3. Given that the observed TO magnitude is by definition matched by the theoretical isochrones to determine the TO age, this discrepancy implies that the absolute magnitude of the RGB-bump in the models is too bright. Realistic uncertainties in the cluster metallicities (and possible He spread within individual clusters associated to the CNO_a abundance anticorrelations) and ages do not erase this difference. A possibility for mitigating the discrepancy is to include overshooting beyond the Schwarzschild boundary of the convective envelope. Convective overshooting decreases the RGB-bump brightness by $\sim 0.8 \text{ mag}/H_p$ (where H_p denotes the local pressure scale height). The discrepancy between theory and observations would disappear with the inclusion of convective overshooting of the order of ~ 0.25 below the Schwarzschild boundary of the convective envelope.

2.3 Tip of the RGB

The tip of the RGB (TRGB) marks the He-ignition in electron degenerate cores of low mass stars. The TRGB bolometric magnitude is weakly dependent on the initial stellar mass, hence the isochrone age, for ages above ~ 5 Gyr. This is because at a given initial chemical composition, the TRGB level is determined by the He-core mass at the He-flash, that is fairly constant in this age range. The core mass decreases for increasing metallicity, while the TRGB bolometric luminosity increases because of the increased efficiency of the H-burning shell, that compensates for the reduced core mass. When

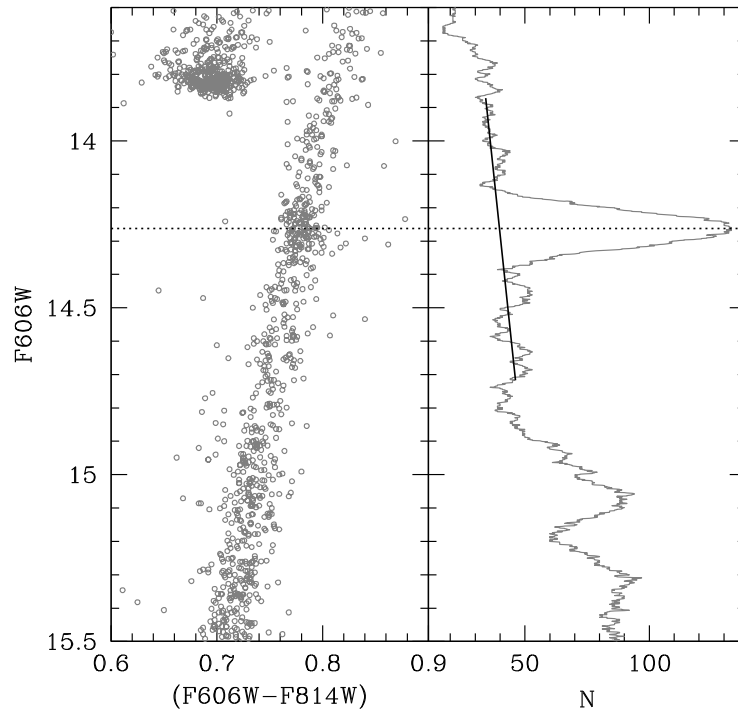


Figure 2. The RGB-bump in the LF (right panel) obtained from GC photometric observations (left panel).

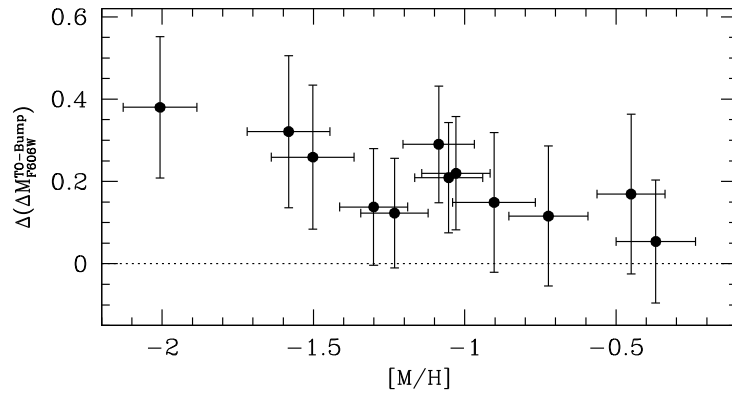


Figure 3. Difference between the values of $\Delta V_{\text{TO}}^{\text{bump}}$ expected from the cluster TO ages, and measured values, as a function of the total metallicity $[M/H]$.

considering the TRGB magnitude in a photometric system, the behaviour of the bolometric correction to the I-band as a function of $[M/H]$ and effective temperature compensates for the variation of the bolometric luminosity with metallicity. The net effect is that $M_{\text{I}}^{\text{TRGB}}$ is predicted to be basically constant at values around $M_{\text{I}}^{\text{TRGB}} = -4$ in the Cousins filter, with both age – for ages above 4–5 Gyr – and metallicity – for $[M/H]$ below ~ -0.7 – as displayed in Fig. 4. This is the reason why the I-band magnitude of the TRGB has been one of the standard candles of choice for stellar systems harbouring old populations. In other photometric bands the dependence of the TRGB absolute magnitude on metallicity (and age) is stronger.

Ageing Low Mass Stars: From Red Giants to White Dwarfs

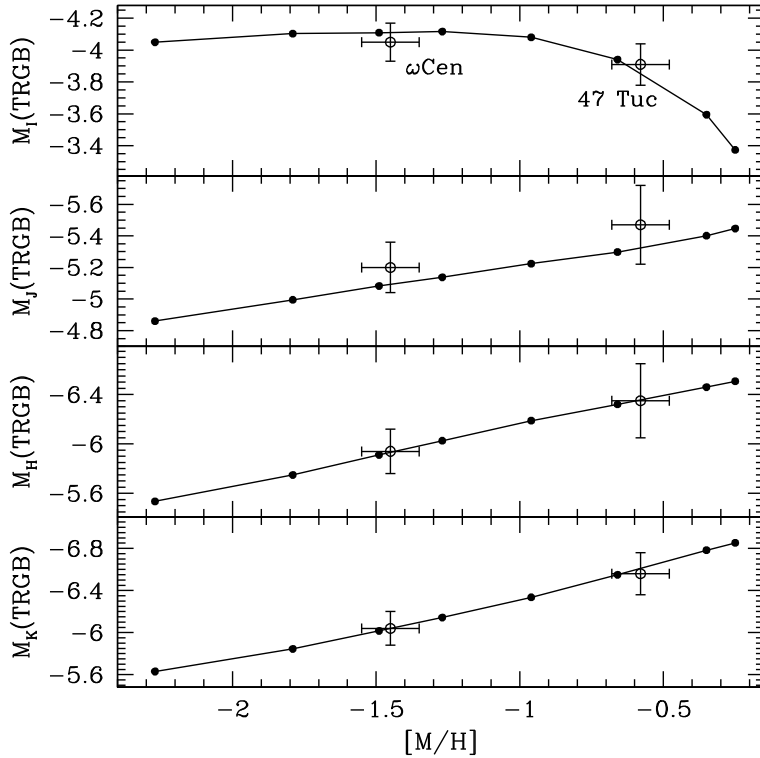


Figure 4. TRGB magnitude in several photometric filters as a function of $[M/H]$ for a typical GC age of 12 Gyr. Empirical estimates for Ω Cen and 47Tuc are plotted with the estimated error bars.

Figure 4 shows the good agreement existing between modern theoretical predictions – that include recent advances in the determination of the $^{14}\text{N}(p, c)^{15}\text{O}$ reaction rate and electron conduction opacities – for a typical GC age ([12]), and empirical estimates of the TRGB magnitude in different photometric bands for the Galactic GCs Ω Cen and 47Tuc ([7]). The cluster distances used in the empirical calibration are consistent with the values determined for eclipsing binaries in both clusters ([35] and [34]). This agreement highlights the reliability of TRGB He-core masses predicted by modern stellar evolution models and as a consequence, also the Zero Age HB theoretical predictions.

2.4 White Dwarf sequences

The comparison of star cluster TO and White Dwarf (WD) ages has very recently confirmed the efficiency of a new physical process at work in the interior of WDs. HST observations of the well populated WD cooling sequence in the old metal rich (metallicity about twice solar) open cluster NGC6791 have produced a deep LF that displays a sharp cut-off at low luminosities, caused by the finite age of the cluster, plus a secondary peak at higher luminosities ([3], [4]) as shown in Fig. 5. The secondary peak is best explained by a $\sim 30\%$ fraction of unresolved WD+WD binary systems, the progeny of a $\sim 50\%$ primordial binary fraction. For the distance estimated from isochrone fitting – consistent with the distance modulus more recently obtained from eclipsing binaries hosted by the cluster ([9]) – the age inferred from the absolute magnitude of the faint cut-off is ~ 6 Gyr, about 2 Gyr younger than the TO age. This age discrepancy disappears with the inclusion in the WD theoretical calculations of the ^{22}Ne diffusion in the liquid phase, a physical process previously neglected in WD model computations, and efficient in WDs originated from high-metallicity progenitors ([18]). The ^{22}Ne

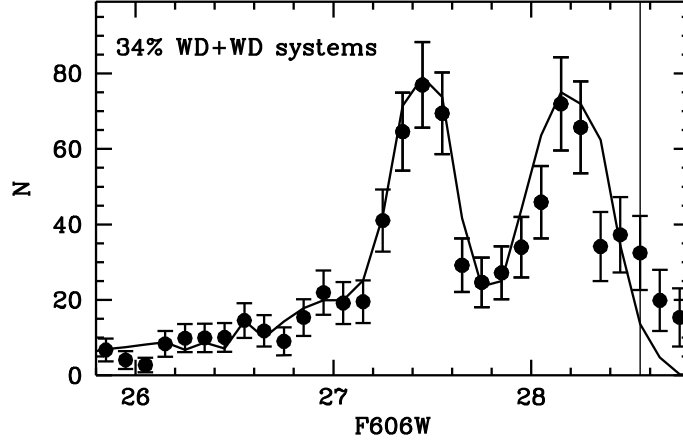


Figure 5. Observed WD luminosity function of NGC6791. Over-imposed is the theoretical counterpart for an age of 6 Gyr and the labeled fraction of unresolved WD + WD binaries.

in the WD cores is produced by He captures on the ^{14}N left from H-burning via the CNO cycle. Because of its two excess neutrons relative to the predominant $A = 2Z$ nuclei, a downward force $\approx 2m_p g$ is exerted on ^{22}Ne nuclei in the WD cores. This forces ^{22}Ne to settle towards the WD centre during the liquid phase. Sinking is stopped at the crystallization boundary. The variation of the ^{22}Ne abundance provides additional energy through the term

$$\left(\frac{LE}{LX_{^{22}\text{Ne}}} \right)_{T,V} \frac{dX_{^{22}\text{Ne}}}{dt} \quad (1)$$

that enters the WD energy generation coefficient. Here E is the internal energy per unit mass, $V = 1/q$, and $dX_{^{22}\text{Ne}}$ the mass fraction of ^{22}Ne .

3. SPECTROSCOPIC DIAGNOSTICS

Spectroscopic estimates of surface chemical abundances in GC stars belonging to different evolutionary stages, have disclosed ongoing shortcomings in our treatment of element transport in stellar interiors.

3.1 Chemical abundances from the TO to the RGB

Atomic diffusion is an additional element transport mechanism – together with convection – that needs to be included in model computations for the Sun, to satisfy the helioseismic constraints. On the other hand, atomic diffusion cannot be fully at work in GC stars, according to abundance measurements from the TO to the RGB in M4 ([24]) and NGC6397 ([20]). Figure 6 displays as an example the case of Fe (an element not involved in the CNONa abundance anticorrelation pattern) in M4 ($[\text{Fe}/\text{H}] \sim -2.0$). Models including atomic diffusion predict a Fe abundance at the TO lower than the initial value (because of Fe diffusion below the convective envelope during the MS) and an increase back to almost the initial value along the RGB, because the deepening of surface convection during the first dredge-up brings back to the surface almost all Fe previously diffused towards the centre. Observations show instead a flat Fe trend with T_{eff} , that points to an inhibition of atomic diffusion from the convective envelope. A partial inhibition of atomic diffusion is also necessary to match the behaviour of heavy element abundances in the more metal poor cluster NGC6397 ($[\text{Fe}/\text{H}] \sim -2.0$). This has been modelled following the ‘turbulent mixing’ formalism by [28], e.g. by adding a properly calibrated additional diffusion coefficient to the term in the diffusion equation that is proportional to the abundance gradient of chemical species. An

Ageing Low Mass Stars: From Red Giants to White Dwarfs

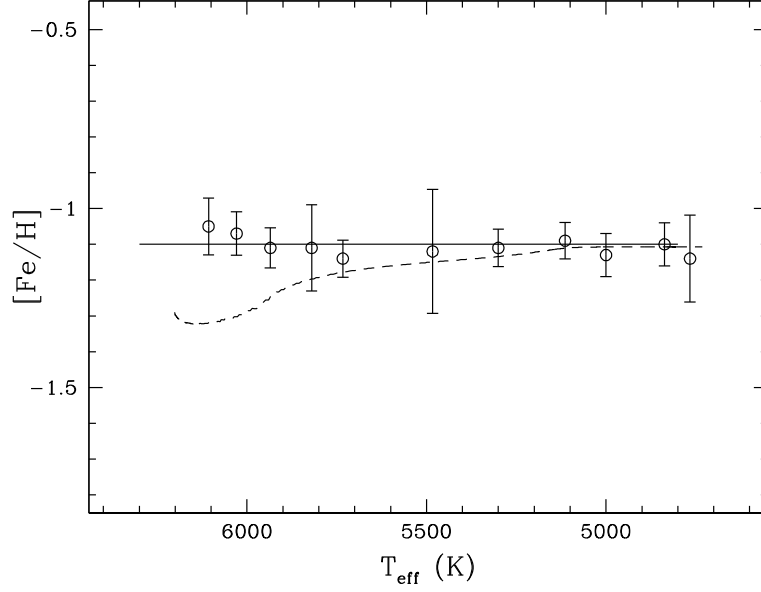


Figure 6. Mean observed $[\text{Fe}/\text{H}]$ values in 11 T_{eff} bins, and associated errors, for a large sample of stars in the Galactic GC M4, from the TO to the lower RGB. Solid and dashed lines display the predictions of an isochrone including diffusion, with initial $[\text{Fe}/\text{H}] = -1.1$ (solid line) after an age of 11 Gyr (dashed line).

example is given by

$$D_{\text{turb}} = 400D_{\text{He}}(T_0) \left[\frac{q}{q(T_0)} \right]^{-3} \quad (2)$$

that represents a turbulent mixing coefficient that is 400 times larger than the He atomic diffusion coefficient at a given temperature T_0 and varies as ρ^{-3} . The temperature T_0 is a free parameter that is tuned to adjust the region where this turbulent mixing is efficient. In practice, this corresponds to enhancing the diffusion term that opposes the creation of chemical gradients in radiative zones. Data for NGC6397 are reproduced for $\log(T_0) \sim 6.0$.

3.2 Chemical abundances along the RGB

Numerous observations in GC and field halo RGB stars (see, i.e., [1], [19]) provide compelling evidence of a mixing process that occurs when low-mass stars reach the RGB bump brightness along the RGB. At this stage, the surface carbon isotopic ratio drops, together with the abundances of lithium and carbon, while that of nitrogen increases slightly. Thermohaline mixing has been identified as the mechanism that should be the cause of these abundance variations. This additional transport mechanism is induced by the molecular weight inversion created by the ${}^3\text{He}({}^3\text{He}, 2p){}^4\text{He}$ reaction in the external wing of the advancing H-burning shell. This reaction converts two particles into three and decreases the mean molecular weight. The instability is expected to set in after the H-burning shell has crossed the H-abundance discontinuity left over by the first dredge-up, and starts moving in a region of uniform composition. At this stage the small molecular weight inversion due to ${}^3\text{He}$ burning affects the chemical profile and enables thermohaline instability to set in. Formally, the thermohaline instability occurs in a stable stratification that satisfies the Ledoux criterion for convective instability,

$$\nabla_{\text{ad}} - \nabla + \left(\frac{\varphi}{\delta} \right) \nabla_{\mu} > 0, \quad (3)$$

but the molecular weight decreases with depth:

$$\nabla_{\mu} := \frac{d \ln \mu}{d \ln P} < 0 \quad (4)$$

with $\nabla = (\partial \ln T / \partial \ln P)$, $\varphi = (\partial \ln \rho / \partial \ln \mu)_{P,T}$ and $\delta = -(\partial \ln \rho / \partial \ln T)_{P,\mu}$, ∇_{μ} and ∇_{ad} being the molecular weight gradient and the adiabatic gradient, respectively.

The element transport is treated as a diffusive process, with diffusion coefficient (that multiplies the chemical abundance gradients) equal to

$$D_t = C_t K \left(\frac{\varphi}{\delta} \right) \frac{-\nabla_{\mu}}{(\nabla_{\text{ad}} - \nabla)} \quad \text{for } \nabla_{\mu} < 0, \quad (5)$$

where K is the thermal diffusivity, and

$$C_t = \frac{8}{3} \pi^2 \alpha^2, \quad (6)$$

with α a free parameter. A value $C_t=1000$ is necessary to reproduce the observational constraint ([15]).

Recent hydrodynamics simulations ([36]) suggest however a much smaller value of C_t , of the order of 10, that would be largely insufficient to reproduce the observed post RGB-bump abundances.

3.3 Chemical abundances along the HB

Photospheric chemical abundances on the Horizontal Branch (HB) of Galactic GCs show striking variations with T_{eff} . Above $T_{\text{eff}} \sim 11500$ K He is underabundant and Fe, Ti, P, Cr Mn, Ni are enhanced by factors ≈ 100 compared to cooler HB stars ([5]). The most straightforward explanation is that these anomalies develop through atomic diffusion processes, in particular gravitational settling and radiative levitation. However, the abrupt disappearance of strong abundance anomalies as one moves below ~ 11500 K suggests that another factor plays an important role. In fact the only existing HB models that include self-consistently gravitational settling and radiative levitation ([21]) predict the onset of abundance anomalies at T_{eff} well below 11000 K.

A recent analysis ([26]) has addressed the observed correlation between the onset of abundance anomalies and surface rotation velocities $v \text{ sini}$ for HB stars in a sample of Galactic GCs ([5], [6]). HB stars hotter than ~ 11000 K have $v \text{ sini}$ below $\sim 5 \text{ km s}^{-1}$, while at each T_{eff} lower than this limit stars display a large range of $v \text{ sini}$, up to $\sim 40 \text{ km s}^{-1}$. First calculations ([26]) show that the dependence of abundance anomalies observed on the HB on T_{eff} can be explained by atomic diffusion transport if one introduces the competition of meridional circulation with the observed T_{eff} dependence of the surface rotation velocity of HB stars. The prediction is that for stars cooler than ~ 11000 K, with high surface rotation velocities, meridional circulation is able to inhibit the effect of atomic diffusion.

4. CONCLUSIONS

It should have transpired from this short review, how photometric and spectroscopic observations of old star cluster are continuing to provide crucial constraints to stellar evolution models of low mass stars. Recent results from the *Kepler* mission are opening a new avenue for model testing in old clusters. Observations of non-radial oscillations in red giants belonging to NGC6791 have provided mass and radius of a sample of RGB stars, by employing the large frequency separation and the frequency of maximum power ([2]). These values agree extremely well with the predictions from the isochrones that best fit the cluster CMD ([4]). An additional important result is the determination of the mass of He-burning stars in the same cluster, that has allowed a direct estimate of the total amount of mass lost along the RGB of this metal rich cluster ([22]). The future of old star clusters as bench tests of low-mass stellar models is bright.

References

- [1] Angelou, G. C., Stancliffe, R. J., Church, R. P., Lattanzio, J. C., & Smith, G. H. 2012, *ApJ*, **749**, 12
- [2] Basu, S., Grundahl, F., & Stello, D. et al. 2011, *ApJ*, **729**, L10
- [3] Bedin, L. R. et al. 2005, *ApJ*, **624**, L45
- [4] Bedin, L. R. et al. 2008, *ApJ*, **678**, 1279
- [5] Behr, B. B. 2003a, *ApJS*, **149**, 67
- [6] Behr, B. B. 2003b, *ApJS*, **149**, 101
- [7] Bellazzini, M., Ferraro, F. R., Sollima, A., Pancino, E., & Origlia, L. 2004, *A&A*, **424**, 199
- [8] Böhm-Vitense, E. 1958, *Zeitschrift für Astrophysik*, **46**, 108
- [9] Brogaard, K., Bruntt, H., Grundahl, F., et al. 2011, *A&A*, **525**, A2
- [10] Carretta, E., Bragaglia, A., Gratton, R., & Lucatello, S. 2009, *A&A*, **505**, 139
- [11] Cassisi S., & Salaris, M. 1997, *MNRAS*, **285**, 593
- [12] Cassisi S., & Salaris, M. 2013, 'Old stellar populations: How to study the fossil record of galaxy formation', Wiley, in press
- [13] Cassisi, S., Salaris, M., & Irwin, A. W. 2003, *ApJ*, **588**, 862
- [14] Cassisi S., Marin-Franch A., Salaris M., Aparicio A., Monelli M., & Pietrinferni A., 2011, *A&A*, **527**, A59
- [15] Charbonnel, C., & Lagarde, N. 2010, *A&A*, **522**, A10
- [16] Frogel, J. A., Cohen, J. G., & Persson, S. E. 1983, *ApJ*, **275**, 77
- [17] Fusi Pecci, F., Ferraro, F. R., Crocker, D. A., Rood, R. T., & Buonanno, R. 1990, *A&A*, **238**, 9
- [18] Garcia-Berro, E et al. 2010, *Nature*, **465**, 194
- [19] Gratton, R. G., Sneden, C., Carretta, E., & Bragaglia, A. 2000, *A&A*, **354**, 169
- [20] Korn, A. J., Grundahl, F., & Richard, O. et al. 2007, *ApJ*, **671**, 402
- [21] Michaud, G., Richer, J., & Richard, O. 2007, *ApJ*, **670**, 1178
- [22] Miglio, A., Brogaard, K., & Stello, D. et al. 2012, *MNRAS*, **419**, 2077
- [23] Mucciarelli, A., Ferraro, F. R., Origlia, L., & Fusi Pecci, F. 2007, *AJ*, **133**, 2053
- [24] Mucciarelli, A., Salaris, M., & Lovisi, L. et al. 2011, *MNRAS*, **412**, 81
- [25] Puzia, T. H., Kissler-Patig, M., Thomas, D. et al. 2005, *A&A*, **439**, 997
- [26] Quievy, D., Charbonneau, P., Michaud, G. & Richer, J. 2009, *A&A*, **500**, 1163
- [27] Renzini, A. 2008, *MNRAS*, **391**, 354
- [28] Richard, O., Michaud, G., & Richer, J. 2005, *ApJ*, **619**, 538
- [29] Salaris, M., & Cassisi, S. 2008, *A&A*, **487**, 1075
- [30] Salaris M., & Weiss A., 2002, *A&A*, **388**, 492
- [31] Salaris, M., Cassisi, S., & Weiss, A. 2002, *PASP*, **114**, 375
- [32] Salaris, M., Weiss, A., & Percival, S. M. 2004, *A&A*, **414**, 163
- [33] Sandage, A., & Schwarzschild, M. 1952, *ApJ*, **116**, 463
- [34] Thompson, I. B., Kaluzny, J., & Pych, W. et al. 2001, *AJ*, **121**, 3087
- [35] Thompson, I. B., Kaluzny, J., Rucinski, S. M., et al. 2010, *AJ*, **139**, 329
- [36] Traxler, A., Garaud, T., & Stellmach, S. 2011, *ApJ*, **728**, L29